First-principles theory-based scaling of the SOL width in limited tokamak plasmas, experimental validation, and implications for the ITER start-up

P. Ricci[1], F.D. Halpern[1], J. Loizu[1], S. Jolliet[1], A. Mosetto[1], F. Riva[1], C. Wersal[1], A. Fasoli[1], I. Furno[1], B. Labit[1], F. Nespoli[1], C. Theiler[1], G. Arnoux[2], J.P. Gunn[3], J. Horacek[4], M. Kočan[5], B. LaBombard[6] and C. Silva[7]

[1]Ecole Polytechnique Fédérale de Lausanne (EPFL), Centre de Recherches en Physique des Plasmas CH-1015 Lausanne, Switzerland
[2]CCFE, Culham Science Centre, Abingdon, Oxon, OX14 3DB, UK
[3]CEA, IRFM, 13108 Saint-Paul-lez-Durance, France
[4]Institute of Plasma Physics AS CR, v.v.i., Za Slovankou 1782/3, 182 00, Praha 8, Czech Republic
[5]ITER Organization, Route de Vinon-sur-Verdon, 13115 Saint-Paul-lez-Durance, France
[6]Massachusetts Institute of Technology, Cambridge, MA 02139, USA
[7] Instituto de Plasmas e Fusão Nuclear, Instituto Superior Técnico, Universidade de Lisboa, Portugal

Corresponding Author: paolo.ricci@epfl.ch

Abstract:

The steady-state heat load onto the plasma facing components of tokamak devices depends on the SOL width, which results from a balance between plasma outflowing from the core region, turbulent transport, and losses to the divertor or limiter. Understanding even the simplest SOL configurations, like circular limited plasmas, is a stepping-stone towards more complicated configurations, with important implications for the ITER start-up and ramp-down phases. Here we present a first-principle based scaling for the characteristic SOL pressure scale length in circular, limited tokamaks that has been obtained by evaluating the balance between parallel losses at the limiter and non-linearly saturated resistive ballooning mode turbulence driving anomalous perpendicular transport. It is found that the SOL width increases with the tokamak major radius, the safety factor, and the density, while it decreases with the toroidal magnetic field and the plasma temperature. The scaling is benchmarked against the flux-driven non-linear turbulence simulations that have been carried out with the GBS code. This code solves the drift-reduced Braginskii equations and evolves self-consistently plasma equilibrium and fluctuations, as the result of the interplay between the plasma injected by a source, which mimics the plasma outflow from the tokamak core, the turbulent transport and the plasma losses to the vessel. GBS has been subject to a verification and validation procedure unparalleled in plasma physics. The theoretical

scaling reveals good agreement with experimental data obtained in a number of tokamaks, including TCV, Alcator C-MOD, COMPASS, JET, and Tore Supra.

1 Introduction

The steady-state heat load onto the plasma facing components of tokamak devices depends on the scrape-off layer (SOL) width [**?**, **?**, **?**, **?**], which results from a balance between plasma outflowing from the core region, turbulent transport, and losses to the divertor or limiter. Understanding SOL plasma dynamics is crucial for ITER and beyond, as the heat load on the vessel constrains the lifetime of its components. Understanding even the simplest SOL configurations, like circular limited plasmas, is critical as this is a stepping stone towards more complicated configurations and it has important implications for the ITER start-up and ramp-down phases [**?**].

The GBS code has been developed in the last few years to simulate plasma turbulence in SOL conditions [**?**]. This code solves the drift-reduced Braginskii equations for low-frequency turbulence [**?**], avoiding the assumption of small amplitude plasma turbulence with respect to the equilibrium quantities. Therefore, the code evolves self-consistently plasma equilibrium and fluctuations, as the result of the interplay between the plasma injected by a source, which mimics the plasma outflow from the tokamak core, the turbulent transport and the plasma losses to the vessel. GBS has been subject to a verification and validation procedure unparalleled in plasma physics. The verification of the correct implementation and solution of the model equations has been performed by using the method of manufactured solutions [**?**] and GBS simulations of the TORPEX basic plasma physics experiment have been successfully validated against Langmuir probe data using a rigorous methodology [**?**].

A detailed study of the interaction of the plasma with the solid wall has been carried out in order to implement correctly the physics of this region in GBS [**?**]. The plasma wall interaction has been modeled by using a fully kinetic code and, based on the kinetic results, a set of boundary conditions has been found that have been implemented in GBS at the sheath edge, where the drift-reduced Braginskii model loses its validity.

Thanks to the GBS simulations and analytical investigations, we have reached an understanding, among others, of the mechanisms leading to SOL turbulent saturation [**?**], the SOL turbulent regimes [**?**], the role of electromagnetic effects [**?**, **?**], the mechanisms determining the SOL electrostatic potential [**?**], the phenomena responsible for the the SOL intrinsic toroidal rotation [**?**], and the role of finite aspect ratio effects [**?**].

The present work reports on a theory-based scaling of the SOL characteristic pressure radial scale length $L_p = -p/\nabla p$ at the outboard mid-plane of an inboard limited plasma. The SOL width results from a power balance between parallel losses and anomalous transport due to low frequency interchange turbulence. Our work concentrates on a relatively simple, circular, inner-wall limited configuration.

2 The GBS system of equations

At the plasma edge, where collisionality plays a dominant role and kinetic effects such as particle trapping and wave-particle resonance are less important, fluid modelling is still an appropriate choice to perform global turbulence simulations at a computational cost that allows a wide parameter scan. We adopt the drift ordering, which is based on assuming that $d/dt \ll \omega_{ci}$ and that turbulence is essentially aligned with the field-line, $|\nabla_\parallel| \ll |\nabla_\perp|$. Within the drift ordering, it is useful to split the analysis of the dynamics into the direction parallel and perpendicular to the magnetic field, by decomposing $\mathbf{V}_\alpha = V_{\parallel\alpha}\mathbf{b} + \mathbf{v}_{\perp\alpha}$, and expressing $\mathbf{v}_{\perp\alpha}$ as the sum of $E \times B$, diamagnetic, and polarization drifts. Using this expression for the plasma velocity, it is possible to derive the equations that are solved by GBS. Within this derivation, we consider the cold ion approximation, $T_i \ll T_e$, neglecting p_i effects.

The model implemented in the GBS code is constituted by the continuity equation, the vorticity equation, Ampere's law, the equation for the ion and electron parallel motion, and the equation for the electron temperature:

$$\frac{\partial n}{\partial t} = -\frac{R}{\rho_{s0}}\frac{1}{B}[\phi, n] + \frac{2n}{B}\left[C(T_e) + \frac{T_e}{n}C(n) - C(\phi)\right]$$
$$-n(\mathbf{b}\cdot\nabla)V_{\parallel e} - V_{\parallel e}(\mathbf{b}\cdot\nabla)n + \mathcal{D}_n(n) + S \tag{1}$$

$$\frac{\partial \omega}{\partial t} = -\frac{R}{\rho_{s0}}\frac{1}{B}[\phi, \omega] - V_{\parallel i}(\mathbf{b}\cdot\nabla)\omega + B^2\left[(\mathbf{b}\cdot\nabla)(V_{\parallel i} - V_{\parallel e})\right.$$
$$\left.+\frac{(V_{\parallel i} - V_{\parallel e})}{n}(\mathbf{b}\cdot\nabla)n\right]$$
$$+2B\left[C(T_e) + \frac{T_e}{n}C(n)\right] + \frac{B}{3n}C(G_i) + \mathcal{D}_\omega(\omega) \tag{2}$$

$$\frac{\partial V_{\parallel e}}{\partial t} + \frac{m_i}{m_e}\frac{\beta_e}{2}\frac{\partial \psi}{\partial t} = -\frac{R}{\rho_{s0}}\frac{1}{B}[\phi, V_{\parallel e}] - V_{\parallel e}(\mathbf{b}\cdot\nabla)V_{\parallel e} - \frac{m_i}{m_e}\frac{2}{3}(\mathbf{b}\cdot\nabla)G_e$$
$$-\frac{m_i}{m_e}\nu(V_{\parallel e} - V_{\parallel i}) + \frac{m_i}{m_e}(\mathbf{b}\cdot\nabla)\phi - \frac{m_i T_e}{n m_e}(\mathbf{b}\cdot\nabla)n$$
$$-1.71\frac{m_i}{m_e}(\mathbf{b}\cdot\nabla)T_e + \mathcal{D}_{V_{\parallel e}}(V_{\parallel e}) \tag{3}$$

$$\frac{\partial V_{\parallel i}}{\partial t} = -\frac{R}{\rho_{s0}}\frac{1}{B}[\phi, V_{\parallel i}] - V_{\parallel i}(\mathbf{b}\cdot\nabla)V_{\parallel i} - \frac{2}{3}(\mathbf{b}\cdot\nabla)G_i$$
$$-\left[(\mathbf{b}\cdot\nabla)T_e + \frac{T_e}{n}(\mathbf{b}\cdot\nabla)n\right] + \mathcal{D}_{V_{\parallel i}}(V_{\parallel i}) \tag{4}$$

$$\frac{\partial T_e}{\partial t} = -\frac{R}{\rho_{s0}}\frac{1}{B}[\phi, T_e] - V_{\parallel e}(\mathbf{b}\cdot\nabla)T_e + \frac{4}{3}\frac{T_e}{B}\left[\frac{7}{2}C(T_e) + \frac{T_e}{n}C(n) - C(\phi)\right]$$
$$+\frac{2T_e}{3}\left[0.71(\mathbf{b}\cdot\nabla)V_{\parallel i} - 1.71(\mathbf{b}\cdot\nabla)V_{\parallel e} + 0.71\frac{(V_{\parallel i} - V_{\parallel e})}{n}(\mathbf{b}\cdot\nabla)n\right]$$
$$+\mathcal{D}_{T_e}(T_e) + \mathcal{D}_{T_e}^\parallel(T_e) + S_T \tag{5}$$

which are coupled to Ampère's law, $\nabla_\perp^2 \psi = n(V_{\parallel i} - V_{\parallel e})$, and to the Poisson equation $\nabla_\perp^2 \phi = \omega$. We also note that diffusion operators $\mathcal{D}$ and $\mathcal{D}^\parallel$ have been introduced for numerical purposes: GBS allows the choice between standard diffusion and/or fourth-order hyperdiffusion operators.

The curvature operator, $C = B/2[\nabla \times (\mathbf{b}/B)]$, the perpendicular Laplacian operator, $\nabla_\perp^2$, the parallel gradient, $\mathbf{b} \cdot \nabla$, and the Poisson bracket, $[A, B] = \mathbf{b} \cdot (\nabla f \times \nabla g)$, that appear in Eqs. (**??-??**), have to be specified for each geometry; this is made easy by the GBS modular coding. The complete expression of these operators can be found in Ref. [**?**]. Herein we focus on tokamak SOL with circular flux surfaces in the infinite aspect ratio limit.

3   Estimate of the SOL width

Recent studies using the GBS code have shown that the magnitude of the turbulent fluxes in the SOL can be predicted using the non-linear local flattening of the pressure profile caused by the linear modes [**?, ?**], the so-called gradient removal mechanism. Here, we summarize the results of this saturation model, which is fully derived in [**?**]. In non-linear, flux-driven simulations, it is observed that turbulent saturation occurs when the pressure non-linearity exhausts the linear drive from the background gradient, i.e. $\tilde{p}/\overline{p} \sim \sigma_r/L_p$. (The tilde and the overbar indicate background and perturbed quantities, respectively, and σ_r is radial extension of the mode.) In the regime of interest here, $k_\theta L_p > 1$ (k_θ is the poloidal wavenumber), it can be shown that σ_r is determined by combining turbulent (k_θ^{-1}) and equilibrium (L_p) spatial scales, $\sigma_r \simeq \sqrt{L_p/k_\theta}$. Consequently, our model specifically deals with the turbulent saturation of meso-scale structures such as the ones inferred from experimental measurements. We also note that σ_r is not affected by magnetic shear, in the typical parameter range of limited discharges. Using the leading order contribution of the continuity equation, $\partial_t p + \nabla_\perp \cdot (\mathbf{v}_{E \times B} p) = 0$, it is possible to relate the pressure and electrostatic potential fluctuations assuming that the $E \times B$ shear flow is negligible, i.e. $\gamma \tilde{p}/\overline{p} \sim k_\theta \tilde{\phi}/(BL_p)$, where γ is the linear growth rate of the instability that dominates the non-linear dynamics. Therefore, the time-averaged radial $E \times B$ turbulent flux, $\Gamma = \left\langle k_\theta \tilde{p} \tilde{\phi} \right\rangle_t /B$, can be estimated as $\Gamma \sim \tilde{p}\gamma/k_\theta$. The balance between perpendicular turbulent transport, $\nabla_\parallel(pv_{\parallel e}) \sim \overline{p}c_s/(qR)$, and the parallel losses at the sheath, $\nabla_\parallel(pv_{\parallel e}) \sim \overline{p}c_s/(qR)$, leads to an estimate of the profile length

$$L_p \sim (qR/c_s)(\gamma/k_\theta)_{\max} \tag{6}$$

where R is the tokamak major radius, $q \simeq (r/R)B_\phi/B_\theta$ is the cylindrical tokamak safety factor, and $c_s = \sqrt{T_i + T_e}/m_i$ is the sound speed. In deriving Eq. (**??**), it is assumed that the flux is driven by a single mode that leads to the flattest possible pressure profile. Furthermore, it is assumed that parallel temperature gradients are weak. This assumption breaks down in high-density low-temperature discharges, where parallel temperature gradients develop and the effect of neutral particles becomes more important.

The pressure gradient length can now be computed assuming that SOL turbulence is driven by resistive ballooning modes (RBMs). Non-linear, 3D electromagnetic simulations

have addressed the nature of SOL turbulence in limited circular plasmas, finding that RBMs dominate the plasma dynamics [**?**]. The SOL is very collisional compared to the plasma core, and, in the absence of magnetic field line periodicity, RBMs are dominant over non-linearly driven drift waves; at the same time linearly unstable drift waves are efficiently damped by the magnetic shear.

Therefore, in order to obtain L_p through equation (**??**), we now seek for the typical growth rate and poloidal wave length of RBMs. A simple dispersion relation for RBMs, valid in the low β limit and considering only the low-field side mid-plane region (where the curvature drive for the modes is strong), can be obtained from the reduced resistive magnetohydrodynamic (MHD) equations. It gives that $\gamma \sim \gamma_b = c_s\sqrt{2/(RL_p)}$ and $k_\theta^2 \sim (\nu_0\sigma_\parallel v_a^2)(1-\alpha)/(q^2R^2\gamma_b)$. Introducing these estimates into Eq. (**??**), we obtain

$$\tilde{L}_p\tilde{R}^{-1/2} = [2\pi\alpha_d(1-\alpha)^{1/2}/q]^{-1/2} \tag{7}$$

where $\tilde{L}_p$ and $\tilde{R}$ are L_p and R normalized to $\rho_s = \sqrt{m_i(T_i+T_e)}/(eB)$, the adimensionalized parameter $\alpha_d = 2^{-3/4}\nu^{-1/2}(R/L_p)^{1/4}/(2\pi q)$ measures the strength of the parallel damping of the resistive ballooning mode, while $\alpha = q^2\beta R/L_p$ is the ideal ballooning stability parameter.

Equation (**??**) is particularly amenable for comparisons with the flux-driven non-linear turbulence simulations carried out with the GBS code. The drift-reduced Braginskii model used for the simulations does not separate fluctuations from the background profiles, and no separation between equilibrium and turbulent length scales is imposed a priori. The plasma density, temperature, potential, and parallel velocities are initialized using smooth profiles with a small perturbation superimposed. Plasma sources, which mimic the plasma outflow from the core, are then introduced. The pressure gradient increases until linearly unstable modes appear, driving turbulence that leads to perpendicular transport. Over a longer period, the modes saturate and a non-linear turbulent steady state is achieved. Since interchange turbulence and sheared flows occur in the simulated plasma, blob dynamics are also present in the simulations. The plasma gradients are naturally reached as a balance between plasma injection, turbulent transport, and parallel losses at the plasma sheaths. Therefore, the GBS code is especially suited for verifying the dimensionless scaling given by Eq (**??**).

An extensive simulation campaign, the details of which will be published in a longer paper, was carried out to investigate the inner-wall limited SOL parameter space. In essence, we are interested in simulating limited plasmas where RBMs dominate transport and to maximize the range of the dimensionless parameter space probed. The resistivity and q are varied to investigate the effect of the parallel dynamics of the turbulent modes. The plasma β is increased by several orders of magnitude to test the strength of electromagnetic effects. Crucially, the normalized major radius $\tilde{R}$ is increased by a factor of 4 in order to test the effects of the plasma size predicted by the scaling. The results are shown in Fig. 1. Overall, good agreement is found between the non-linear simulation results and the prediction of the analytical theory over the entire parameter range. This is due to the fact that the non-linear turbulent spectra observed in GBS simulations are typically dominated by a few resonant long wavelength modes with $k_\theta\rho_s \sim 0.1$. Furthermore, sec-
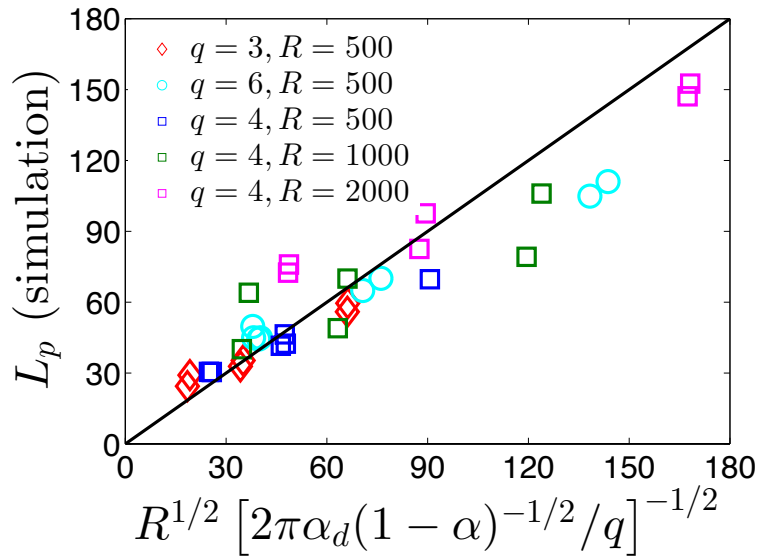
FIG. 1: *Dimensionless pressure gradient length $\tilde{L}_p$ s shown as a function of the dimensionless parameters α, α_d, $\tilde{R}$, and q, according to Eq. (??). All the parameters (except for q, which is imposed) are self consistently obtained in the GBS simulations.*

ondary instabilities, such as the Kelvin-Helmholtz mode, do not to play a significant role saturating SOL turbulence in the regime of interest here.

It is also possible to obtain a scaling in terms of engineering parameters. This is a more practical approach for comparing against experimental data and to extrapolate L_p to future devices. Since β is very small in the SOL of circular limited plasmas, we take the electrostatic limit $\alpha \ll 1$, which leads to the following scaling:

$$L_p \simeq 7.22 \times 10^{-8} q^{8/7} R^{5/7} B_\phi^{-4/7} T_{e0}^{-2/7} n_{e0}^{2/7} \left(1 + \frac{T_{i0}}{T_{e0}}\right) \qquad (8)$$

Here q, n_0, T_{e0}, and T_{i0} must be provided at the low-field-side midplane of the last closed flux surface (LCFS), while R and B_ϕ must be provided at the magnetic axis. All quantities are expressed using SI units except for T_{e0} and T_{i0}, which are given in eV. The constant factor arises from the Spitzer conductivity, and we have approximated the Coulomb logarithm $\ln \Lambda \simeq 15$. The factor of $q^{8/7} \sim I^{-8/7}$ results in a strong dependence of L_p on the plasma current, while the explicit dependence on T_e, T_i, and n is rather weak.

In parallel with the ITPA effort, we have carried out a comparison of the theoretical and simulation results against experimental data from several tokamaks worldwide (TCV, Alcator C-Mod, Tore Supra, JET, COMPASS) [?]. This comparison yielded good agreement (see Fig. 2). The scaling developed has implications to the ITER start-up and ramp-down phases [?]. On this respect, we remark that we have been able to explain theoretically [?] the difference that is observed between low- and high-field side limited discharges [?, ?].

Detailed comparisons with gas puff imagining and turbulence probe measurements from Alcator C-Mod and TCV are currently being carried out, the effect of shaping (e.g.,
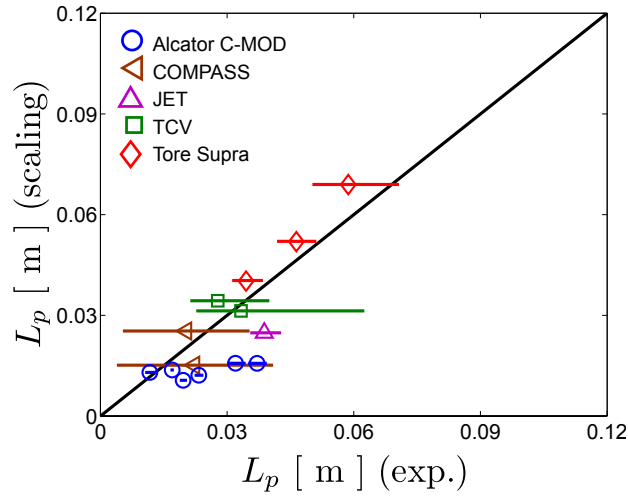
FIG. 2: Scaling given by equation ?? is compared against experimental data from inner-wall limited discharges. The abscissa and ordinate provide, respectively, the experimental data and the prediction of the theoretical scaling. The horizontal bars indicate the 95% confidence interval obtained from the fitting of L_p. ITER start-up predictions are displayed as down-triangles.

elongation and triangularity) on the SOL width is being analysed, as well as the role of neutral particle physics. We are also approaching the study of narrow pressure scale length that has been observed in the near SOL of a number of tokamak devices, and which can also have consequences for the plasma start-up and ramp-down in ITER.

References

[1] W. Fundamenski et al, Nucl. Fusion 51 (2011) 093028.

[2] T. Eich et al, Phys. Rev. Lett. 107 (2012) 215001.

[3] J. Gunn et al, J. Nucl. Mater. 438 (2013) S184.

[4] M.A. Makowski et al, Phys. Plasmas 19 (2012) 056122.

[5] G. Arnoux et al, Nucl. Fusion 53 (2013) 073016.

[6] P. Ricci et al, Plasma Phys. Contr. Fusion 54 (2012) 124047.

[7] A. Zeiler et al, Phys. Plasmas 5 (1998) 2654.

[8] F. Riva et al, Phys. Plasmas 21 (2014) 062301.

[9] P. Ricci et al, Phys. Plasmas 18 (2011) 032109.

[10] J. Loizu et al, Phys. Plasmas 19, (2012) 122307.

[11] P. Ricci et al., Phys. Plasmas 20 (2013) 010702.

[12] A. Mosetto et al., Phys. Plasmas 20 (2013) 092308.

[13] F.D. Halpern et al., Phys. Plasmas 20 (2013) 052306.

[14] F.D. Halpern et al., Nuclear Fusion 54 (2014) 043003.

[15] J. Loizu et al., Plasma Phys. Contr. Fusion 55 (2013) 124019.

[16] J. Loizu et al., Phys. Plasmas 21 (2014) 062309.

[17] S. Jolliet et al., Phys. Plasmas 21 (2014) 022303.

[18] F.D. Halpern et al., Nuclear Fusion 53 (2013) 122001.

[19] J. Loizu et al., Nuclear Fusion 54 (2014) 083033.

[20] C. Silva et al, J. Nucl. Mater. 438 (2013) S189.

[21] M. Kočan et al, Plasma Phys. Contr. Fusion 52 (2012) 045010.